Article

Not peer-reviewed version

Distorted Oxygen Environments of Titanium in Phosphate Crystals and Glasses – A Discussion of Scattering Results

Uwe Hoppe *

Posted Date: 9 June 2026

doi: 10.20944/preprints202606.0673.v1

Keywords: X-ray scattering; neutron scattering; phosphate glass; atomic structure; titanium dioxide; second-order Jahn-Teller theorem; range of glass formation

 doi:10.20944/preprints202606.0673.v1

Article

Distorted Oxygen Environments of Titanium in Phosphate Crystals and Glasses—A Discussion of Scattering Results

Uwe Hoppe

Institute of Physics, Rostock University, 18051 Rostock, Germany; uwe.hoppe@uni-rostock.de

Abstract

Our earlier X-ray and neutron scattering data on TiO_2-P_2O_5 glasses with minor Al_2O_3 impurities are re-examined with some modification. Then, it is compared with recent results. There, it is reported that triply coordinated oxygens in the TiO_6 octahedra cause unusual distortions. Here, these effects are discussed more thoroughly. Triply coordinated oxygens enforce short cation-cation distances. The associated repulsions drive distortions, which are facilitated by the second-order Jahn-Teller effect of the d^0 transition element Ti^{4+}. The Ti^{4+} cations shift away from their octahedral centers. It is compared with GeO_2-P_2O_5 glasses. The size of Ge is similar to that of Ti, but a GeO_6 unit does not suffer distortions. According to these specifics, different ranges of glass formation are observed.

Keywords: X-ray scattering; neutron scattering; phosphate glass; atomic structure; titanium dioxide; second-order Jahn-Teller theorem; range of glass formation

1. Introduction

Some titano-phosphates—such as the potassium titano-phosphate crystal—have attracted considerable interest for optical applications due to their large nonlinear refractive indices [1]. This property was assigned to the distortions of the oxygen environments of Ti. In the $KTiO(PO_4)$ crystal, some Ti–O–Ti bridges are out of balance and consist of a short and a long bond [2]. This difference was interpreted using the second-order Jahn-Teller (SOJT) theorem [1]. More generally, the distortions of the MO_6 octahedra (M – transition metal with a d^0 configuration) lowering its symmetry were described as out-of-center shifts of the M sites [3]. The empty *d* orbitals of M mix with occupied *p* orbitals of the oxygen ligands, and the shifts of M avoid the nearly degenerate states. The smaller the energy gap between the orbitals, the stronger the tendency to the out-of-center shift of M. V^{5+} and Mo^{6+} were classified as strong distorters, which never occur in undistorted MO_6 octahedra [3,4]. The moderate distorters Ti^{4+}, Nb^{5+}, and Ta^{5+}, and W^{6+} can form undistorted MO_6 octahedra, but unbalanced outer forces cause an out-of-center shift of M against only slight resistance. The shift of an M is directed to octahedral corners, edges, or faces, accompanied by characteristic changes in the M–O bond lengths (see Figure S1). For example, the oxygens of the TiO_6 in crystalline $PbTiO_3$ [5] form a nearly regular octahedron, but the Ti^{4+} is shifted by 0.033 nm toward one of the corners.

It is known that Ti^{4+} cations form TiO_4 or TiO_5 units in addition to the TiO_6 units, for example, in silicate glasses [6]. The ratios of the ionic radii for a given atom A surrounded by spherical oxygen ligands determine which polyhedra are preferably formed [7]. Ratios r_A/r_O of 0.414 or 0.225 correspond to exactly filling the gaps within octahedra or tetrahedra. The corresponding ratios for Ti^{4+} and O^{2-} are 0.45 and 0.31, respectively, as calculated from the ionic radii [8], indicating a preference for octahedral units. The slightly smaller Ge^{4+} has ratios of 0.39 and 0.29. GeO_4 tetrahedra are preferred, and vitreous GeO_2 consists of a continuous network of such units, but GeO_6 octahedra are also known in several crystals and glasses. The Ti-centered oxygen polyhedra could differ in silicate and phosphate environments. Si–O bonds in SiO_4 units possess bond valences of about 1.0 v.u. (valence units), while the P–O bonds in bridges with neighboring M have larger bond valences

 doi:10.20944/preprints202606.0673.v1

[9], which vary with the connectivity of the phosphate network and local constraints (see Figure S1). Hence, Ti–O bonds of bond valences <1.0 v.u. occur and favor TiO_5 or TiO_6 units.

If large ranges of scattering vector magnitude (Q) are used in scattering experiments on glasses, then details about different bond lengths, in addition to the mean coordination numbers, are obtained. Such experiments on TiO_2-containing glasses were performed on silicate and phosphate systems [10–15]. The scattering contrast of Ti atoms is changed by isotopic substitution in neutron scattering experiments [10–12]. Another profitable approach is the contrast change when combining X-ray and neutron scattering data [14,15].

The study of the Ti environments in glasses is restricted to distributions of Ti–O pair distances. Detailed geometries of the Ti-centered oxygen polyhedra, as available for crystals, are not accessible for glass structures. The total Ti–O coordination number gives the average of the frequencies of the TiO_4, TiO_5, and TiO_6 units. The known Ti–O distances of the polyhedra of related crystals support the analysis. Considering the crystals' coordination polyhedra indicates a problem. Well-defined bond lengths for the structural groups are not observed due to the strong TiO_6 distortions. The empirical relationship between bond valence and bond length, as introduced by Brown & Altermatt [16], is a helpful tool. Here, more recent parameters for the Ti–O distances are used [17].

In this work, our previous scattering results for TiO_2-P_2O_5 glasses with minor Al_2O_3 impurities [15] are re-examined and partially modified. This is necessary for the subsequent comparison with recent results on binary TiO_2-P_2O_5 glasses [14]. Although slight interactions between the TiO_x and AlO_4 units for the glasses in [15] cannot be ruled out, it is useful to consider these data together. They complement each other in the TiO_2/P_2O_5 ratio. Small Al_2O_3 contents extend the range of glass formation. Furthermore, the out-of-center shifts of the Ti positions within their oxygen octahedra, as predicted for this d^0 transition element by SOJT, were not discussed for glass structures at that time [15]. The comparison with the GeO_2-P_2O_5 glasses [18], Ge is a main-group element with fully occupied d orbitals, highlights the role of the SOJT effects.

2. Materials and Methods

The experiments have been described in [15]. Here, only the essential parameters of the experiments are repeated. The quasi-binary titano-phosphate glasses have compositions $54TiO_2$-$40P_2O_5$-$6Al_2O_3$ and $61TiO_2$-$35P_2O_5$-$4Al_2O_3$. The samples contain sufficient oxygen to avoid P–O–P bridges. AlO_4 tetrahedra are expected in the presence of isolated PO_4. To a good approximation, both samples are quasi-binary glasses with TiO_2 contents of 61.4 and 66.3 mol%, respectively, after subtracting a suitable $AlPO_4$ content. The samples are labelled TP60 and TP65 as in [15]. Atomic number densities ϱ_T of 74.1 and 74.4 atoms/nm³ were calculated from the mass densities. X-ray diffraction was performed at the BW5 beamline of the DORIS III synchrotron at the German Electron Synchrotron (Hamburg), and neutron diffraction at the GEM instrument of the ISIS spallation source at the Rutherford Appleton Laboratory (Chilton, UK). The upper limits of the magnitude of scattering vector, Q_{max}, are 280 nm^{-1} (X-rays) and 500 nm^{-1} (neutrons), where Q is calculated from the scattering angle, 2θ, and the radiation wavelength, λ by $Q = (4\pi/\lambda)\sin\theta$.

3. Results

The static structure factors $S(Q)$ were obtained from the normalized scattering intensities as shown in [15]. The short-range order parameters of the glasses are determined from the real-space correlation functions $T(r)$, which are obtained from $S(Q)$ by Fourier transformation with

$$T(r) = 4\pi r\rho_T + 2/\pi \int_0^{Q_{max}} Q[S(Q) - 1]\sin(Qr)dQ \quad . \qquad (1)$$

Different from [15] and in accordance with [14], damping is not used. The values of Q_{max} used for the X-ray and neutron scattering data are 250 and 360 nm^{-1}, respectively, to exclude noisy scattering intensities at high Q-ranges. The $T(r)$ curves are shown in Figure 1.

 doi:10.20944/preprints202606.0673.v1

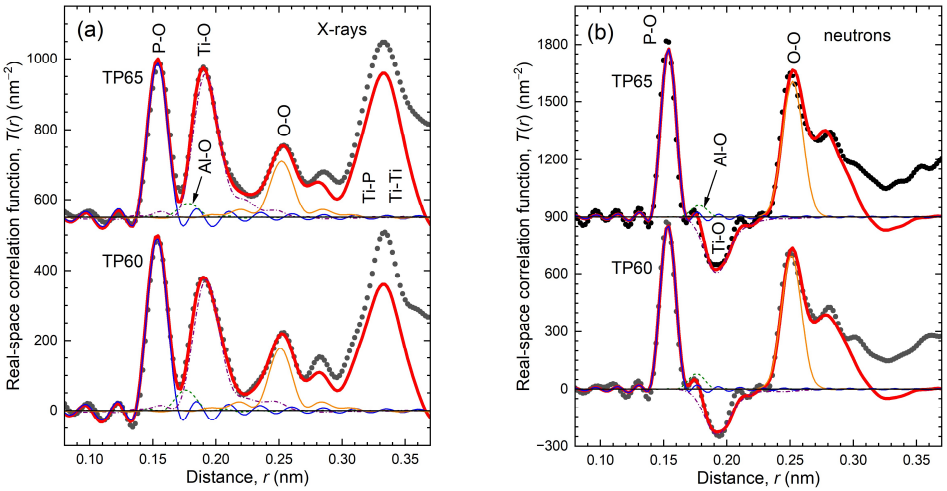

Figure 1. Real-space correlation functions of the TiO_2-P_2O_5 glasses [15] in the range of the first-neighbor peaks calculated by Equation 1 using the (a) X-ray and (b) neutron scattering data (dotted lines). The model functions (red solid lines) are obtained by parameter fits. Distinct model peaks are given with thin lines for P–O distances (blue solid lines), Al–O distances (green dashed lines), Ti–O distances (purple dash-dotted lines), and the shortest O–O distances (orange solid lines). For better clarity, the baselines of the TP65 curves have been shifted upwards.

The Q_{max} limits in the Fourier integral (Equation 1) cause a peak broadening and termination ripples. These effects are taken into account during parameter fitting according to the convolution method of Mozzi & Warren [19,20]. Fits were made simultaneously to the X-ray and neutron $T(r)$ functions, which helps separate the Al–O, Ti–O, and O–O correlations in the distance range $0.17 < r < 0.25$ nm. The Ti–O weighting factors change strongly for the X-ray and neutron correlations. The peak of the Ti–O distances appears as a minimum (cf. Figure 1b) due to the negative neutron scattering length of Ti in natural isotopic abundance. Compared to X-ray scattering, the O–O correlation is significantly enhanced in neutron scattering.

Gaussian functions approximate the distance peaks. Their parameters are the coordination number N_{ij}, the distance r_{ij}, and the full width at half maximum (fwhm) Δr_{ij}. The Δr_{ij} of a Gaussian is related to the root of the mean square deviation σ_{ij} by $\Delta r_{ij} = 2.335\ \sigma_{ij}$. A single Gaussian function is used for the P–O peak, corresponding to the four equivalent bonds in isolated PO_4 tetrahedra. Only these units have been detected by ^{31}P-NMR spectroscopy [21]. A next small single Gaussian approximates the Al–O peak. Three Gaussians are needed to model the Ti–O first-neighbor distances. The shortest O–O distances at ~0.251 nm can be assigned to the edges of the PO_4 units. The edge lengths of the AlO_4 and TiO_6 units are only slightly longer than those of the PO_4. Thus, the next Gaussian in the O–O correlation overlaps with the first one. Different from [15], the N_{OO} value of the first Gaussian is fixed to 3.1, as reported for the X-ray data in [14]. The use of identical N_{OO} parameters in the $T(r)$ model peaks for the X-ray and neutron scattering data requires the assumption of a small fraction of Ti–O distances near 0.24 nm. The Gaussians at ~0.192 and ~0.214 nm describe the main part of the Ti–O peak. The parameters obtained from the fits are listed in Table 1. The large peak in the X-ray $T(r)$ function at ~0.33 nm is approximated by four P–Ti and three Ti–Ti pairs.

The TiO_2 and Al_2O_3 components of both samples provide sufficient oxygen for all PO_4 to exist as isolated units. The parameters of the Al–O peaks are close to those known for crystalline $AlPO_4$ with Al–O distances of 0.174 nm and $N_{AlO} = 4$ [22]. There, all oxygens are in Al–O–P bridges. The parameters of the Ti–O peaks can be compared with those of the related crystals $Ti_5O_4(PO_4)_4$ [23], $Ti_2O(PO_4)_2$ [24], $Ti(P_2O_7)$ [25], and TiO_2 [26] (Brookite). The $Ti_5O_4(PO_4)_4$ structure shows the most strongly distorted TeO_6 units with Ti–O bond lengths ranging from 0.174 to 0.26 nm. The total N_{TiO} values of the glasses are 6.0 ± 0.2 (TP60) and 5.7 ± 0.2 (TP65). The first O–O peak at 0.252 nm with N_{OO} = 3.1 exceeds the calculated coordination numbers of 2.94 (TP60) and 2.72 (TP65), assuming that only

 doi:10.20944/preprints202606.0673.v1

the oxygen edges of the PO_4 units contribute to this peak. Thus, the edges of other oxygen polyhedra are involved in this first Gaussian component of the O–O correlation.

Table 1. Parameters of the Gaussian functions used in simultaneous fits of both $T(r)$ functions obtained from the X-ray and neutron scattering data.

Atom pair	Coordination number, N_{ij}	Distance, r_{ij} (nm)	Fwhm, Dr_{ij} (nm)
TP60 (~61 mol% TiO_2)	3.95 ± 0.10	0.1533 ± 0.0010	0.013 ± 0.001
P–O	4.5 ± 1.0	0.176 ± 0.005	0.014 ± 0.002
Al–O	5.20	0.1925 ± 0.002	0.0235
Ti–O	0.40	0.214*	0.030*
	0.40	0.240*	0.030*
O–O	3.10	0.251	0.0185
	2.70*	0.276*	0.030*
TP65 (~66 mol% TiO_2)	3.95 ± 0.10	0.1537 ± 0.0010	0.0125 ± 0.001
P–O	4.6 ± 1.0	0.178 ± 0.005	0.014 ± 0.002
Al–O	4.60	0.1915 ± 0.002	0.022
Ti–O	0.90	0.214*	0.030*
	0.20	0.250*	0.035*
O–O	3.10	0.252	0.019
	2.70*	0.278*	0.030*

* The parameters marked with asterisks were optimized by hand and then fixed in the final fits.

4. Discussion

4.1. Total Ti–O Coordination Number and Density Behavior

In this chapter, the Ti phosphate glasses with small Al_2O_3 impurities [15] are considered quasi-binary glasses, then with TiO_2 fractions of 61.4 (TP60) and 66.3 (TP65) mol%. The Al_2O_3 is assumed to be bound in $AlPO_4$-like structures. Regarding the P/O ratio, $AlPO_4$ corresponds to a $60TiO_2$-$40P_2O_5$ glass, which is close to that of sample TP60. Figure 2a compares the total Ti–O coordination numbers. To ensure comparability with the N_{TiO} values from [14], distances ≥0.24 nm are also disregarded for our values (cf. Table 1). The latter values of TP60 and TP65 are given as small circles. The N_{GeO} values for binary GeO_2-P_2O_5 glasses [18], the GeP_2O_7 [27], and $Ge_5O(PO_4)_6$ [28] crystals are added for comparison. They exemplify the behavior of a main-group A^{4+} cation of similar size.

The coordination behavior of Ti and Ge differs significantly, although single Ti–O bonds (0.182 nm) are only slightly longer than single Ge–O bonds (0.175 nm) [13,17,18]. The N_{GeO} values follow a curve called M_{TO}, given by $M_{TO} = 2(x + 1)/x$, until the range of glass formation ends at x = ~0.8. A change in N_{GeO} according to M_{TO} indicates a network structure with exclusively doubly coordinated oxygens. This behavior is also realized in the crystals TiP_2O_7 [24] and $Ti_2O(PO_4)_2$ [25]. For $x < 0.7$, the N_{TiO} values of the TiO_2-P_2O_5 glasses show a similar trend, but with a significant upward offset. Finally, the N_{TiO} values start to increase for $x > 0.7$. The relation $N_{TiO} > M_{TO}$ indicates fractions of triply coordinated oxygen, thus, oxygen with either three Ti neighbors or one P and two Ti neighbors. A model for the evolution of the corresponding oxygen fractions is detailed in [14]. It is noteworthy that the number of short Ti–O distances in the glass sample TP60 (5.2 at 0.192 nm) corresponds well with the respective M_{TO} value (circle with hatched fill in Figure 2a). In other words, the oxygens in the glassy network of TP60 seem almost doubly coordinated if only the strong bonds are considered. Is Zachariasen's rule [29] on the exclusion of triply coordinated oxygen in oxide glass networks violated only by elongated bonds? It is unclear whether this also applies to the glasses with higher TiO_2 contents. Analyzing this effect is difficult for the other samples. For sample TP65, the number of short Ti–O bonds is lower than the M_{TO} value. However, there is a significant overlap with the second distance component, as is also the case for the Ti–O peaks of the samples reported in [14].

 doi:10.20944/preprints202606.0673.v1

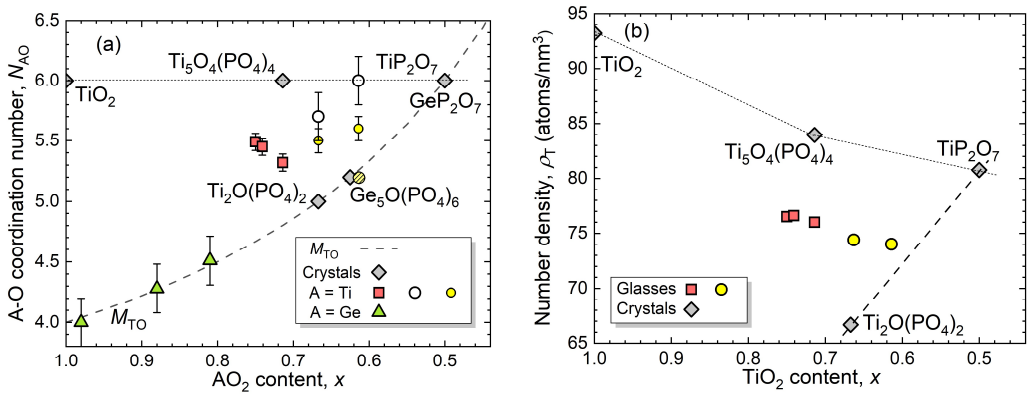

Figure 2. The evolution of the (a) coordination numbers N_{AO} of AO_2-P_2O_5 glasses and crystals and (b) the corresponding number densities of atoms. (a) The N_{GeO} values are taken from [18], the N_{TiO} values from [14] (squares) and [15] (circles – this work). The small circles indicate values where the Ti–O distances of ~0.24 nm have been disregarded. The M_{TO} function (dashed line) follows a model in which all oxygen atoms have two atomic neighbors. For sample TP60, the first distance component at 0.192 nm is indicated by a circle with a hatched fill. (b) The various polymorphs of TiP_2O_7 are known to have different densities. Here, a crystal with a medium density value is chosen [25].

Figure 2b shows the evolution of the number densities of the titano-phosphate materials. The number densities of atoms in crystals with constant N_{TiO} = 6 increase with increasing x, which is attributed to an increasing fraction of triply coordinated oxygen and exchange of tetrahedral PO_4 for octahedral TiO_6 units. On the other hand, if the networks avoid triply coordinated oxygen, then TiO_6 units change to TiO_4, and the number densities decrease. Apart from a definite offset, the ρ_T values of the glasses follow the density trend of those crystals, which are accompanied by fractions of triply coordinated oxygen. Evidently, the number of terminal oxygen atoms (M_{TO}) per Ti does not play a decisive role in the structure of the TiO_2-P_2O_5 glasses. The opposite was established for the GeO_2-P_2O_5 glasses (cf. Figure 2a) [18].

4.2. Details of the Ti–O Bond Lengths

The scattering data are of sufficient quality to discuss detailed shapes of the Ti–O distance peaks. The Ti–O peaks in Figure 3a are calculated using the parameters obtained from the fits (Table 1 in this work and Table VII in [14]). In these comparisons, the radial distribution function (RDF) is used with $RDF(r) = r \cdot T(r)$. Then, the peak area is related to the number of atomic neighbors. For the crystal structures in Figure 3b, Δr_{TiO} values are chosen similar to those of the glasses. Two effects are visible. The mixture of TiO_4 and TiO_6 units in $Ti_2O(PO_4)_2$ [24] causes shorter bond lengths than in TiP_2O_7 [25], where all Ti are exclusively located in TiO_6 units. Both crystals possess only doubly coordinated oxygen. The other two crystal structures show significant components of lengths $r_{TiO} > 0.210$ nm. The brookite [26] shows only a small effect. All oxygens are triply coordinated. However, the TiO_6 octahedra are connected asymmetrically along their edges, causing the Ti position to shift slightly away from the TiO_6 center [3]. On the other hand, only one of the five Ti positions in the $Ti_5O_4(PO_4)_4$ crystal [23] has six equal Ti–O bond lengths. The other four TiO_6 units exhibit strong 1+4+1 deformations (Ti shifts toward a corner - one short, four medium, and one long bond). Three of these Ti sites have an occupancy of only 90%. The remaining Ti atoms occupy even more distorted octahedral sites. Since the latter sites cause only a marginal change, they have been neglected when calculating the Ti–O peak.

 doi:10.20944/preprints202606.0673.v1

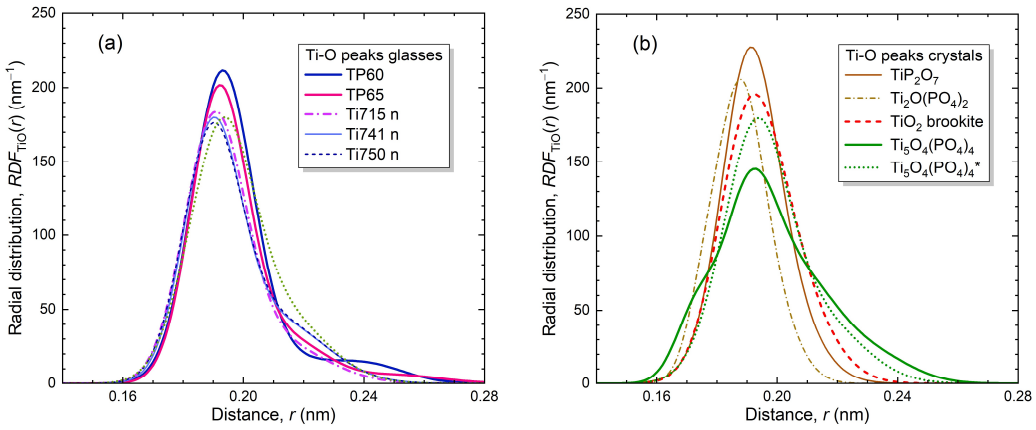

Figure 3. Comparison of the Ti–O distance peaks calculated from (a) the Gaussian function's parameters obtained by fitting the peaks in the real-space correlations of the glasses and (b) the distances taken from related crystal structures [23–26]. The glasses denoted Tixxx n are calculated by the fit parameters taken from the neutron data in [14]. The xxx denotes the TiO_2 fraction 0.xxx. TP60 and TP65 have TiO_2 fractions of 0.614 and 0.663. For the crystals, widths Δr_{TiO} similar to those of the glasses are used. The dotted-lined curve as plotted in both figures belongs to a modified variant of the $Ti_5O_4(PO_4)_4$ crystal (see text).

The origin of the strong TiO_6 distortions in crystalline $Ti_5O_4(PO_4)_4$ lies in a mixture of 70% doubly coordinated and 30% triply coordinated oxygens, as emphasized in [14]. As calculated by the sophisticated structural model for TiO_2-P_2O_5 glasses [14], the fraction of triply coordinated oxygens increases with the TiO_2 content at the expense of doubly coordinated sites. In this process, the number of triply coordinated Ti–O–Ti_2 sites increases at the expense of P–O–Ti_2. This change results in a decrease in the first peak component, accompanied by an increase in the number of longer distances, as is evident in Figure 3a.

At this point, a closer look at the $Ti_5O_4(PO_4)_4$ crystal [23] is useful, in which a relationship between bond length and bond valence (bv) is employed. It is given by the formula $r_{TiO} = R_0 - \ln(bv) * B$, with R_0 = 0.1819 nm and B = 0.0342 nm [17]. The Ti–O bonds exist in four different configurations. The oxygen atoms occupy bridging Ti–O–Ti and P–O–Ti sites or triply linked Ti–O–Ti_2 and P–O–Ti_2 sites. For simplicity, all P–O bond valences of isolated PO_4 could be fixed to 1.25 v.u. However, the valence of the P–O bond in P–O–Ti_2 has 1.18 v.u. as calculated from the distances. This value is compensated with 1.273 v.u. in the P–O–Ti bridges. For each O site, the remaining bond valence is assumed to be distributed equally among the Ti–O bonds. Figure S2 shows the dependence of bond valences on the length of the Ti–O bond. The four types of Ti–O bonds (in the order as listed above) have bond valences of 1.0, 0.73, 0.67, and 0.41 v.u., which leads to Ti–O distances of 0.182, 0.192, 0.196, and 0.212 nm, respectively. A Ti–O peak is calculated using these lengths and the respective proportions of the crystal's bond types. In Figure 3b, this peak (dotted line) is compared with the broader peak (solid line) calculated from the detailed distances in the crystal. Evidently, knowledge of the nature of the neighboring oxygen sites is insufficient to predict the real distribution of Ti–O distances.

Hence, additional distortions are effective in the $Ti_5O_4(PO_4)_4$ crystal [23]. Strong variations in bond lengths from 0.173 to 0.240 nm occur at oxygen atoms with three Ti neighbors. The variations are large in Ti–O–Ti bridges, while only varying within the limits of the widths Δr_{TiO} used to calculate the Ti–O distances to corners of PO_4 units. The Ti^{4+} cations in TiO_2-P_2O_5 glasses have heterogeneous environments with doubly and triply coordinated oxygens, whereby a P^{5+} as a second neighbor causes much stronger repulsions than a Ti^{4+}. As pointed out in the Introduction chapter, the SOJT effect is of crucial importance [1,3]. Due to external forces, a Ti^{4+} cation can be easily displaced away from the center of its oxygen octahedron against only slight resistance. As a result, the distribution of bond lengths broadens. Due to the lower repulsions, bonds to O with only Ti as a second neighbor are most affected. Ti–O distances near 0.175 nm are absent in the glasses, whereas lengths near 0.24 nm are observed (cf. Figure 3a and

 doi:10.20944/preprints202606.0673.v1

Table 1). In distorted TiO_6 octahedra, all short Ti–O bonds (even two or three) are clearly directed toward one side of the octahedron. Figure 4a shows an example of a TiO_6 octahedron with two short bonds to one side, while the longest bonds point in opposite directions. An analogous behavior of V^{5+} in its oxygen environments was demonstrated for vanadium-phosphate glasses using ab initio molecular dynamics [30]. V^{5+} is likewise a d^0 transition element.

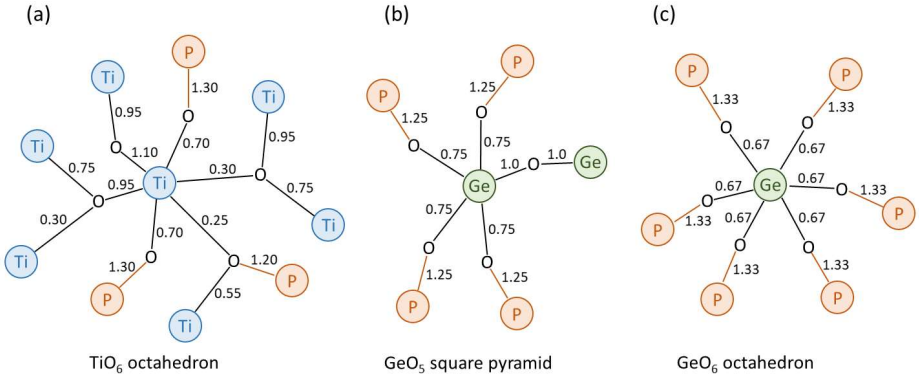

Figure 4. Distributions of bond valences around the Ti^{4+} or Ge^{4+} sites in characteristic structural groups. The numbers given at the bonds are the bond valences in valence units (v.u.). For comparison, the same figure is provided as Figure S3 with bond lengths replacing bond valences (see the supplementary material).

4.3. The Ti–O Units in Different Environments and a Comparison with the Ge–O Units

It appears helpful to compare the behavior of Ti^{4+} and Ge^{4+} cations. The Ge^{4+} cation, similar in size, is free from SOJT effects. Isostructural crystals $KAO(PO_4)$ are known with A = Ti [2] and Ge [31], both in octahedral sites, where Ti–O distances range from 0.172 to 0.216 nm, while Ge–O bonds range from 0.179 to 0.202 nm. The corresponding distance peaks are compared in Figure 5. The TiO_6 units show a 1+4+1 deformation, as already discussed for the $Ti_5O_4(PO_4)_4$ crystal [23]. The GeO_6 unit in $KGeO(PO_4)$ also has significantly varying bond lengths, albeit less pronounced than in the TiO_6 unit. In contrast to the highly asymmetric Ti–O–Ti bridges in $KTiO(PO_4)$ with bond lengths of 0.173 and 0.213 nm [1,2], the bonds in the Ge–O–Ge bridges in $KGeO(PO_4)$ have nearly equal lengths (0.179 and 0.181 nm) [31].

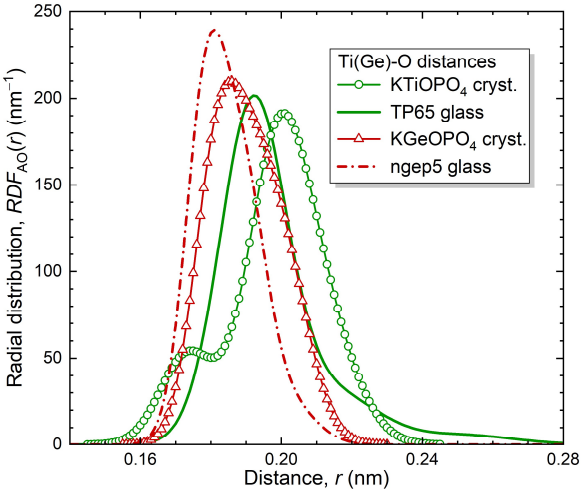

Figure 5. Comparison of the A–O distance peaks (A = Ti, Ge) calculated from the Gaussian function's parameters obtained by fitting the peaks in the real-space correlations of the glasses TiO_2-P_2O_5 TP65 (this work), Na_2O-GeO_2-

 doi:10.20944/preprints202606.0673.v1

P_2O_5 ngep5 [32], and the distances in the $KAO(PO_4)$ crystals (A = Ti, Ge) [2,29]. For the crystals, the widths Δr_{AO} used are similar to those of the glasses.

The A–O peaks of the glasses are shifted to slightly smaller distances. Due to $N_{AO} < 6$ for both glasses, there are small fractions of AO_4 and AO_5 units with shorter bonds. The peaks have equal widths. In contrast to the Ge–O peak, the Ti–O peak shows a significant tail toward long distances. The deformation type of the TiO_6 units in the glasses cannot be specified. A 1+4+1 deformation with a single short bond, such as in the crystal, is not detected in the glasses.

The TiO_5 square pyramid, as in the $Na_2TiOSiO_4$ crystal [33], is a variant of the 1+4+1 deformation, in which the sixth oxygen atom is displaced to a greater distance [3]. The close similarity to the scattering results [10,11] for the K_2O-TiO_2-$2SiO_2$ glasses confirms the existence of such units in silicate glasses (cf. Figure S4), which have also been found in silicate glasses of other similar compositions [6]. A $100KTiPO_5$-$15P_2O_5$-$5SiO_2$ (KTP) glass was studied [15] to find a distorted TiO_6 unit similar to that of the $KTiO(PO_4)$ crystal [2]. This proved unsuccessful, and a nearly symmetrical Ti–O peak from TiO_6 units was obtained (cf. Figure S4).

The SiO_2-rich Ti-silicate glasses provide a suitable environment for Ti^{4+} to form TiO_4 tetrahedra with four single bonds in Si–O–Ti bridges [6,13]. In this case, a TiO_6 octahedron would require triply coordinated oxygen atoms in Si–O–Ti_2 configurations—a feature that appears problematic. This behavior with TiO_4 is not transferable to phosphate glasses. In that case, Ti^{4+} is always confronted with over-bonded P–O bonds ($bv > 1$ v.u., see Figure S1), which then force under-bonded Ti–O linkages resulting in TiO_6 units.

Despite only minor differences in the cationic sizes of A = Ge and Ti — the lengths of their single A–O bonds are 0.175 and 0.182 nm, respectively — their A_2O-P_2O_5 systems exhibit distinctly different tendencies regarding crystal structures and glass formation. The flexibility of distorted TiO_6 octahedra—compared to rather rigid GeO_6 octahedra (cf. Figure 4)—exerts an enormous influence on the structures observed. Potentially strong TiO_6 distortions enable the incorporation of triply coordinated oxygen atoms within the octahedron, resulting in $N_{TiO} > M_{TO}$ and dense packing fractions. Thus, there is a pronounced tendency to octahedral structural units. Figure 4a shows an example of a distorted TiO_6 unit with two short bonds. At the same time, the preferred TiO_6 units, accompanied by an increasing fraction of triply coordinated oxygen, limit glass formation at a TiO_2 content $x > 0.75$ [14]. To explain the values $N_{TiO} < 6$ for the TiO_2-P_2O_5 glasses discussed, some TiO_5 square pyramids must exist. The TiO_5 are similar to the GeO_5 pyramids shown in Figure 4b, which could form in the presence of isolated PO_4 units with bond valences of 1.25 v.u. Triply coordinated oxygens are not needed to participate in the TiO_5.

In contrast to TiO_2-P_2O_5 glasses, GeO_2-P_2O_5 glasses are obtained up to vitreous GeO_2 but are limited to $x > \sim 0.8$ [18] (cf. Figure 2a). The addition of P_2O_5 in the form of isolated PO_4 units is accompanied by an increase in N_{GeO} due to over-bonded P–O bonds (1.25 v.u.) in P–O–Ge bridges. A GeO_5 square pyramid is possible with these PO_4 units, as shown in Figure 4b. What is happening concerning a GeO_6 octahedron? It could use six P–O–Ge linkages with P–O bond valences of 1.33 v.u. (cf. Figure 4c - such as in the GeP_2O_7 crystal [27]) or triply coordinated oxygen neighbors. Otherwise, the sum of bond valences of the Ge would exceed 4.0 v.u. Bond valences of 1.33 v.u. are typical for PO_4 end groups (see Figure S1) [9]. Due to strong repulsions in P–O–Ge_2 configurations, triply coordinated oxygens are not possible in GeO_6 units, which results in $N_{GeO} = M_{TO}$. Due to the dominance of isolated PO_4 in glasses with $x > 0.6$, rigid GeO_6 units are difficult to insert into the networks. This problem is solved in the crystals $Ti_2O(PO_4)_2$ [24] and $Ge_5O(PO_4)_6$ [28] by strong distortions of the isolated PO_4 units. These distortions compensate for the different bond valences required for the AO_4 and AO_6 units, implying significant internal stresses within the PO_4 units—a scenario that is unlikely in glasses. Consequently, GeO_2-P_2O_5 glasses form only within a narrow compositional range close to vitreous GeO_2.

Glasses approaching the composition $50AO_2$-$50P_2O_5$—whether with A = Ti or Ge—are difficult to obtain due to the strong tendency to crystallize to AP_2O_7 forms [25,27] that contain highly

 doi:10.20944/preprints202606.0673.v1

symmetric AO_6 octahedra surrounded by PO_4 end groups (cf. Figure 4c). This tendency toward crystallization is suppressed in ternary Na_2O-GeO_2-P_2O_5 glasses [32]. These glasses, whose compositions predominantly contain PO_4 end groups, are excellently suited for incorporating Ge into GeO_6 octahedra, as illustrated in Figure 4c. A maximum Ge–O coordination number of 5.6 ± 0.4 was observed.

5. Conclusions

Recently, it was shown that the range of glass formation in the $(TiO_2)_x(P_2O_5)_{1-x}$ system is limited to $0.71 < x < 0.75$, whereby triply coordinated oxygens are involved in the glassy networks. Here, the analysis of our scattering data of similar glasses with x = 0.61 and 0.66 – they have small Al_2O_3 impurities – has been repeated, and all results are discussed together.

To achieve agreement between the results of X-ray and neutron scattering, it proved necessary to allow for small proportions of Ti–O distances at ~0.24 nm. Mixtures of TiO_5 and TiO_6 units are observed, whereby the large Ti–O distances belong to highly distorted TiO_6 octahedra. The Ti–O coordination numbers indicate networks of dominantly doubly coordinated oxygens with significant fractions of triply coordinated oxygens in TiO_6 units. Triply coordinated oxygen enforces shorter cation-cation distances than oxygen bridges. The associated repulsion drives distortions. They are then facilitated by the SOJT effects of the d^0 transition element Ti^{4+}, resulting in displacements of Ti^{4+} cations away from the octahedral centers. This is accompanied by asymmetric distributions of bond lengths at oxygens with two or three Ti bonding neighbors.

Given the potential for strong octahedral distortions, Ti favors octahedral oxygen environments but requires specific support to occupy tetrahedral positions. In contrast, the main-group element Ge—which is only slightly smaller than Ti—prefers relatively undistorted octahedral environments that do not accommodate triply coordinated oxygen. Consequently, it forms glass structures containing GeO_6 octahedra only to a limited extent, favoring GeO_4 units instead. The preferences for different oxygen polyhedra in the TiO_2-P_2O_5 and GeO_2-P_2O_5 systems define distinct regions of glass formation.

Supplementary Materials: The following supporting information can be downloaded at the website of this paper posted on Preprints.org, Figure S1: Structural units in titano-phosphates; Figure S2: Empirical relationship between bond valence and bond length for Ti–O distances; Figure S3: Distributions of bond lengths around the Ti^{4+} or Ge^{4+} sites; Figure S4: Comparison of the Ti–O distance peaks.

Funding: This research received no external funding.

Data Availability Statement: The data will be made available upon request.

Conflicts of Interest: The authors declare no conflicts of interest.

References

1. Stucky, G.D.; Phillips, M.L.F.; Gier, T.E. The Potassium Titanyl Phosphate Structure Field: A Model for New Nonlinear Optical Materials. *Chem. Mater.* **1989**, *1*, 492-509.
2. Tordjman, I.; Masse, R.; Guitel, J.C. Structure crystalline du monophosphate $KTiPO_5$. *Z. Kristallogr.* **1974**, *139*, 103-115.
3. Kunz, M.; Brown, I.D. Out-of-Center Distortions around Octahedrally Coordinated d^0 Transition Metals. *J. Solid State Chem.* **1995**, *115*, 395-406. Doi: 10.1006/jssc.1995.1150.
4. Ok, K.M.; Halasyamani, P.S.; Casanova, D.; Llunell, M.; Alemany, P.; Alvarez; S. Distortions in Octahedrally d^0 Transition Metal Oxides: A Continuous Symmetry Measures Approach. *Chem. Mater.* **2006**, *18*, 3176-3183. Doi: 10.1021/cm0604817.
5. Nelmes, R.J.; Kuhs, W.F. The crystal structure of tetragonal $PbTiO_3$ at room temperature and at 700 K. *Solid State Commun.* **1985**, *54*, 721-723. Doi: 10.1016/0038-1098(85)90595-2.

 doi:10.20944/preprints202606.0673.v1

6. Farges, F.; Brown Jr., G.E.; Navrotsky, A.; Gan, H.; Rehr, J.J. Coordination chemistry of Ti(IV) in silicate glasses and melts: II. Glasses at ambient temperature and pressure. *Geochim. et Cosmochim. Acta* **1996**, *60*, 3039-3053. Doi: 10.1016/S0016-7037(97)00050-1.
7. Magnus, A. Über chemische Komplexverbindungen. *Z. anorg. Chemie* **1922**, *124*, 289-321.
8. Shannon, R.D.; Prewitt, C.T. Effective ionic radii in oxides and fluorides. *Acta Cryst. B* **1969**, *25*, 925-946. Doi: 10.1107/S0567740869003220.
9. Brow, R.K. Review: the structure of simple phosphate glasses. *J. Non-Cryst. Solids* **2000**, *263* & *264*, 1-28. Doi: 10.1016/S0022-3093(99)00620-1.
10. Yarker, C.A.; Johnson, P.A.V.; Wright, A.C.; Wong, J.; Greegor,R.B.; Lytle, F.W.; Sinclair,R.N. Neutron diffraction and EXAFS evidence for TiO_5 units in vitreous $K_2O{\cdot}TiO_2{\cdot}2SiO_2$. *J. Non-Cryst. Solids* **1986**, *79*, 117-136. Doi: 10.1016/0022-3093(86)90041-4.
11. Cormier, L.; Gaskell, P.H.; Calas, G.; Soper, A.K. Medium-range order around titanium in a silicate glass studied by neutron diffraction with isotopic substitution. *Phys. Rev. B* **1998**, *58*, 11322-11330. Doi: 10.1103/PhysRevB.58.11322.
12. Martin, R.A.; Moss, R.M.; Lakhkar, N.J.; Knowles, J.C.; Cuello, G.J.; Smith, M.E.; Hanna, J.V.; Newport, R.J. Structural characterization of titanium-doped Bioglass using isotopic substitution neutron diffraction. *Phys. Chem. Chem. Phys.* **2012**, *14*, 15807-15815. Doi: 10.1039/c2cp43032k.
13. Efthimiopoulos, I.; Palles, D.; Richter, S.; Hoppe, U.; Möncke, D.; Wondraczek, L.; Nolte, S.; Kamitsos, E.I. Femtosecond laser-induced transformations in ultra-low expansion glass: Microstructure and local density variations by vibrational spectroscopy. *J. Appl. Phys.* **2018**, *123*, 233105. Doi: 10.1063/1.5030687.
14. Lange, E.G.; Youngman, R.E.; Aitken, B.G.; Ensuncho, L.; Zeidler, A.; Hufziger, K.T.; Lee, S.H.; Cuello, G.J.; Eckert, H.; Salmon, P.S. Titanium phosphate glasses: Beyond tetrahedral network structures. *J. Chem. Phys.* **2025**, *163*, 244501. Doi: 10.1063/5.0301521.
15. Hoppe, U.; Brow, R.K.; Tischendorf, B.C.; Kriltz, A.; Jóvári, P.; Schöps, A.; Hannon, A.C. Structure of titanophosphate glasses studied by X-ray and neutron diffraction. *J. Non-Cryst. Solids* **2007**, *353*, 1802-1807. Doi: 10-1016/j.jnoncrysol.2007.01.079.
16. Brown, I.D.; Altermatt, D. Bond valence parameters obtained from a systematic analysis of the inorganic crystal structure database. *Acta Cryst. B* **1985**, *41*, 244-247. Doi: 10.1107/S0108768185002063.
17. Gagné, O.C.; Hawthorne, F.C. Comprehensive derivation of bond-valence parameters for ion pairs involving oxygen. *Acta Cryst. B* **2015**, *71*, 562-578. Doi: 10.1107/S2052520615016297.
18. Hoppe, U.; Brow, R.K.; Tischendorf, B.C.; Jóvári, P.; Hannon, A.C. Structure of GeO_2-P_2O_5 glasses studied by x-ray and neutron diffraction. *J. Phys.: Condensed Matter* **2006**, *18*, 1847-1860. Doi: 10.1088/0953-8984/18/6/002.
19. Mozzi, R.L.; Warren, B.E. The structure of vitreous silica. *J. Appl. Cryst.* **1969**, *2*, 164-172. Doi: 10.1107/S0021889869006868.
20. Leadbetter, A.J.; Wright, A.C. Diffraction studies of glass structure: I. Theory and quasi-crystalline model. *J. Non-Cryst. Solids* **1972**, *7*, 23-36. Doi: 10.1016/0022-3093(72)90015-4.
21. Brow, R.K.; Tallant, D.R.; Warren, W.L.; McIntyre, A.; Day, D.E. Spectroscopic Studies of the Structure of Titanophosphate and Calcium Titanophosphate Glasses. *Phys. Chem. Glasses* **1997**, *38*, 300-306.
22. Schwarzenbach, D. Die Kristallstruktur von $AlPO_4$ (Tiefquarzmodifikation). *Naturwissenschaften* **1965**, *52*, 343-344. Doi: 10.1007/BF00592009.
23. Reinauer, F.; Glaum, R. Ideal and Real Structure of $Ti_5O_4(PO_4)_4$: X-ray and HRTEM Investigations. *Acta Cryst. B* **1998**, *54*, 722-731. Doi: 10.1107/S0108768198003590.
24. Babaryk, A.A.; Adawy, A.; Garcia, I.; Trobajo, C.; Amghouz, Z.; Colodrero, R.M.P.; Cabeza, A.; Olivera-Pastor, P.; Bazaga-Garcia, M.; dos Santos-Gómez, L. Structural and proton conductivity studies of fibrous π-$Ti_2O(PO_4)_2{\cdot}2H_2O$: application in chitosan-based composite membranes. *Dalton Transact.* **2021**, *50*, 7667-7677. Doi: 10.1039/D1DT00735A
25. Senguttuvan, P.; Rousse, G.; Oró-Solé, J.; Tarascon, J.M.; Palacin, M.R. A low temperature TiP_2O_7 polymorph exhibiting reversible insertion of lithium and sodium ions. *J. Mater. Chem. A* **2013**, *1*, 15284-15291. Doi: 10.1039/C3TA13756B.

 doi:10.20944/preprints202606.0673.v1

26. Baur, W.H. Atomabstände und Bindungswinkel im Brookit, TiO_2. *Acta Cryst.* **1961**, *14*, 214-216. Doi: 10.1107/S0365110X61000747.
27. Kaiser, U.; Glaum, R. Beiträge zum thermischen Verhalten und zur Kristallchemie wasserfreier Phosphate. XI. Darstellung und Kristallstruktur einer triklinen Modifikation von GeP_2O_7. *Z. anorg. allg. Chemie* **1994**, *620*, 1755-1759. Doi: 10.1002/zaac.19946201016.
28. Mayer, H.; Völlenkle, H. Die Kristallstruktur von $Ge_5O(PO_4)_6$. *Monatshefte für Chemie* **1972**, *103*, 1560-1571.
29. Zachariasen, W.J. The Atomic Arrangement in Glass. *J. Am. Ceram. Soc.* **1932**, *54*, 3841-3851. Doi: 10.1021/ja01349a006.
30. Wansi Wendji, S.D.; Massobrio, C.; Boero, M.; Tugène, C.; Levchenko, E.; Shuaib, F.; Piotrowski, R.; Hamani, D.; Delaizir, G.; Geffroy, P.-M.; Thomas, P.; Masson, O.; Bouzid, A.; Ori, G. Quantitative assessment of the structure and bonding properties of $50V_xO_y$-$50P_2O_5$ glass by classical and Born-Oppenheimer molecular dynamics. *J. Non-Cryst. Solids* **2024**, *634*, 122967. Doi: 10.1016/j.jnoncrysol.2024.122967.
31. Voronkova, V.I.; Yanovskii, V.K.; Sorokina, N.J.; Verin, I.A.; Simonov, V.I. Ferroelectric phase transition and crystal structure of $KGeOPO_4$. *Kristallografiya* **1993**, *38*, 147-151.
32. Hoppe, U.; Wyckoff, N.P.; Brow, R.K.; von Zimmermann, M.; Hannon, A.C. Structure of Na_2O-GeO_2-P_2O_5 glasses by X-ray and neutron diffraction. *J. Non-Cryst. Solids* **2014**, *390*, 59-69. Doi: 10.1016/j.jnoncrysol.2014.02.013.
33. Nyman, H.; O'Keeffe, M.; Bovin, J.-O. Sodium titanium silicate, Na_2TiSiO_5. Acta Cryst. B 1978, 34, 905-906. Doi: 10.1107/50567740878014594.